Neogenin interacts with hemojuvelin through its two membrane-proximal fibronectin type III domains[†]

Fan Yang[‡], **Anthony P. West Jr.**[§], **George P. Allendorph**[‖], **Senyon Choe**[‖], and **Pamela J. Bjorkman**[*],[§],[⊥]

[‡]Graduate Option in Chemistry, California Institute of Technology, Pasadena, California 91125

[§]Division of Biology, California Institute of Technology, Pasadena, California 91125

[⊥]Howard Hughes Medical Institute, California Institute of Technology, Pasadena, California 91125;

[‖] Structural Biology Laboratory, The Salk Institute, La Jolla, CA 92037

Abstract

Hemojuvelin is a recently-identified iron-regulatory protein that plays an important role in affecting the expression of hepcidin, a key iron regulatory hormone. Although the underlying mechanism of this process is not clear, several hemojuvelin-binding proteins, including the cell surface receptor neogenin and bone morphogenetic protein (BMP) cytokines, have been identified. The ectodomain of neogenin is composed of four immunoglobulin-like (Ig) domains followed by six fibronectin type III-like (FNIII) domains. Here we report expression of soluble versions of hemojuvelin and neogenin for biochemical characterization of their interaction and the interaction of HJV with BMP-2. Hemojuvelin normally undergoes an autocatalytic cleavage, and as *in vivo*, recombinant hemojuvelin exists as a mixture of cleaved and uncleaved forms. Neogenin binds to cleaved and non-cleaved hemojuvelin, as verified by its binding to an uncleaved mutant hemojuvelin. We localized the hemojuvelin binding site on neogenin to the membrane-proximal fifth and sixth FNIII domains and the juxtamembrane linker, and showed that a fragment containing only this region binds 2-3 orders of magnitude more tightly than the entire neogenin ectodomain. Binding to the most membrane-proximal region of neogenin may play a role in regulating the levels of soluble and membrane-bound forms of hemojuvelin, which in turn would influence the amount of free BMP-2 available for binding to its receptors and triggering transcription of the hepcidin gene. Our finding that BMP-2 and neogenin bind simultaneously to hemojuvelin raises the possibility that neogenin is part of a multi-protein complex at the hepatocyte membrane involving BMP, its receptors, and hemojuvelin.

Iron is a vital nutrient for almost all organisms. The ability to convert between ferric (Fe^{3+}) and ferrous (Fe^{2+}) states allows iron to function as an electron donor and acceptor in many essential biochemical processes (1). However, this feature also makes iron reactive to lipids, proteins and DNA, resulting in damage to cells. Due to its toxicity and indispensability, iron levels in mammals are under tight control. The transferrin/transferrin receptor system is responsible for the regulated delivery of iron to most vertebrate cells (2). In the past decade,

Supporting Information Availables

Figure S1 shows the results of proteolytic digests of the neogenin ectodomain and identification of the endoproteinase Glu-C digested products by western blot and a pull-down assay. Figure S2 shows the data for the determination of the oligomeric state of neogenin FNIII 1-6 using gel filtration chromatography with in-line light scattering. This material is available free of charge via the Internet at http://pubs.acs.org.

other crucial iron-regulatory genes including *HFE* (encoding HFE) (3), *TfR2* (encoding transferrin receptor 2) (4), *SLC40A1* (encoding ferroportin) (5-8),*HAMP* (encoding hepcidin) (9-11), and *HFE2* (encoding hemojuvelin or HJV) (12) have been discovered, and studies of their physiological roles have revealed additional aspects of mammalian iron homeostasis. Mutations in these genes cause hereditary hemochromatosis (HH), characterized by excess absorption and storage of iron in tissues and organs, eventually leading to irreversible organ damage (13).

The gene encoding HJV was identified using a positional cloning strategy in patients with juvenile hemochromatosis (JH) (12). Expressed in fetal and adult liver, heart and skeletal muscle, human HJV is a protein of 426 amino acids, including a hydrophobic N-terminal signal peptide, a conserved RGD tri-amino acid motif, a partial von Willebrandt factor domain, and a glycosylphosphatidylinisotol (GPI) anchor (12). HJV shares sequence similarities with repulsive guidance molecules (RGMs), which are expressed in the central nervous system and function as guidance cues for axons (14,15). HJV and RGMs can undergo auto-cleavage at a conserved Asp-Pro bond (residues 172-173 in human HJV), resulting in two fragments held together by disulfide bond(s) (16,17). Whether this cleavage is required for HJV function(s) is unknown. The lack of an intracellular domain suggests that HJV acts indirectly to influence cellular activities, perhaps through binding to other receptors at the cell surface. Membrane-bound HJV can be released by a furin-like proprotein convertase (18), thus HJV exists in both membrane-bound and soluble forms, giving it the potential to interact with receptors locally and on distant cells.

Disease-causing mutations have been found throughout the HJV sequence (19). Patients with HJV mutations were found to have low concentrations of urinary hepcidin (12), a key iron-regulatory peptide of 20-25 amino acids that is mainly secreted by the liver (10), suggesting that HJV influences hepcidin levels. Consistent with this suggestion, hepcidin mRNA is almost undetectable in HJV$^{-/-}$ mouse hepatocytes (20). Although HJV transcripts were found in high levels in skeletal muscle from healthy individuals (12), no significant developmental abnormalities were observed in HJV$^{-/-}$ mice other than iron overload (20). HJV expression in skeletal muscle is proposed to function to provide a pool of soluble HJV, which competes with the cell-associated form in regulatory pathways (16).

Recent studies revealed that neogenin, an immunoglobulin (Ig) superfamily member that is widely expressed in various tissues including brain, kidney, liver and skeletal muscle (21,22), is a high affinity receptor for RGMs, and that this ligand-receptor complex regulates neuronal survival (14,23). Like its RGM relatives, wildtype HJV (wt HJV) also binds to neogenin, but the most prevalent JH mutant (G320V) does not (17). The extracellular portion of human neogenin is composed of four Ig-like domains and six fibronectin type III (FNIII) repeats, and the intracellular domain contains 13 potential serine/threonine phosphorylation sites (21). A recent study demonstrated that HJV's involvement in regulatory processes is complex, as HJV was also identified to be a co-receptor for bone morphogenetic proteins 2 and 4 (BMP-2 and BMP-4), cytokines that function in various aspects of cell growth, proliferation and apoptosis (24,25). The BMP-HJV interaction was found to trigger hepatic hepcidin expression through the classic BMP signaling pathway (26). It has been proposed that neogenin regulates the ratio of membrane-bound versus soluble HJV, with the soluble form of HJV competing with the membrane-bound form for binding to BMPs (27). How the neogenin-HJV interaction responds to body iron levels and what signaling cascade it receives and/or activates remain to be determined.

In this study, we characterized the interaction between soluble forms of HJV and neogenin by determining the stoichiometry of the complex, its affinity, and the binding epitope on neogenin for HJV. We demonstrated that the HJV-binding epitope of neogenin consists of the two FNIII

domains that are closest to the cell membrane and the juxtamembrane linker. Unexpectedly, a truncated form of neogenin containing only this region bound to HJV with an affinity that was 2-3 orders of magnitude higher than the affinity of the intact neogenin ectodomain for HJV. The differences in equilibrium and kinetic constants for the interaction of HJV with the two forms of neogenin suggested that intact neogenin could exist in two conformations: an HJV-binding conformation mimicked by the truncated FNIII construct and a conformation in which the HJV binding site is occluded. In addition, we demonstrated that BMP-2 and neogenin did not compete for binding to HJV, which is consistent with the observation that neither BMP-2 nor its antagonist affects neogenin-mediated HJV shedding from the cell membrane (28). These results were interpreted in terms of a model in which neogenin binding affects the levels of soluble versus membrane-bound HJV as part of regulating iron homeostasis.

Experimental Procedures

Construction of expression plasmids

Human HJV and neogenin cDNAs were obtained from Caroline Enns at the Oregon Health and Sciences University. The cDNA encoding the ectodomain of HJV (residues 1-401) with a C-terminal 6x-His tag was sub-cloned into the pVL1393 baculovirus transfer vector (BD Biosciences). A non-cleavable HJV mutant D172A, in which residue 172 was changed from aspartate to alanine, was generated using the QuikChange site-directed mutagenesis kit (Qiagen). To make the neogenin ectodomain, DNA encoding the hydrophobic signal sequence (residues 1 – 33), the ectodomain (residues 34 to 1103), and a C-terminal 6x-His tag was PCR-amplified and ligated into pVL1393. Truncated forms of neogenin consisting of the six FNIII repeats (FNIII 1-6, residues 439-1103) and the last two FNIII repeats (FNIII 5-6, residues 851-1103) were generated by applying the Seamless cloning strategy (Stratagene) to the neogenin ectodomain construct such that both preserved the original hydrophobic signal peptide. As in the neogenin ectodomain construct, the ectodomain tail (residues 1062-1103) was also included in these two truncated neogenin constructs. Individual FNIII domains from neogenin were constructed by subcloning the DNA encoding residues 852-961 (FNIII 5) or residues 952-1103 (FNIII 6), each with a C-terminal 6x-His tag, into the pAcGP67A baculovirus transfer vector (BD Biosciences), which includes a gp67 hydrophobic signal peptide. Shorter versions of FNIII 5-6, FNIII 5, and FNIII 6 were constructed using different beginning and ending residues, which were determined using NMR structures of single neogenin FNIII domains (PDB ID: 1×5j and 1×5k). The shorter versions, sFNIII 5-6, sFNIII 5, and sFNIII 6, consisted of residues 853-1054, 853-952, and 952-1054, respectively. All DNA constructs were verified by sequencing.

Expression and purification of recombinant proteins

Recombinant proteins were purified from the supernatants of baculovirus-infected High Five (Hi-5) cells using Ni-NTA and gel filtration chromatography. Neogenin supernatants were exchanged into 50 mM Tris pH 7.4, 150 mM NaCl, and then adjusted to 300 mM NaCl, 10% glycerol, and 10 mM imidazole before being loaded on a Ni-NTA Superflow column (Qiagen). The eluates were then concentrated and loaded onto a Superdex 200 10/30 or Superdex 75 10/30 gel filtration column (GE Healthcare) using a 20 mM Tris pH 7.4, 150 mM NaCl, 2 mM EDTA running buffer. The purification of wildtype and mutant HJV was done similarly, except that the buffers contained a higher concentration of NaCl (300 mM for the first buffer exchange, 500 mM for loading of the Ni-NTA column, and 300 mM for the gel filtration column). Human BMP-2 was expressed in *E. coli* as inclusion bodies, purified and refolded as described (29).

Proteolysis of neogenin

Neogenin FNIII 1-6 was incubated with trypsin (Sigma), papain (Sigma), endoproteinase Glu-C (Sigma), thermolysin (Sigma) or thrombin (Roche) at various enzyme-to-substrate ratios in

buffers selected according to the manufacturers' instructions (100 mM Tris-acetate pH 7.6, 100 mM Bis-Tris pH 6.5, 100 mM Tris pH 8.0, 50 mM Tris pH 8.0 and 50 mM Tris pH 7.4, respectively). All reactions were stopped by incubation at 100°C for 5 min. Digested products were analyzed on 11% SDS-PAGE gels and visualized by staining with Coomassie blue (Bio-rad). For Western blot analyses, the gels were electroblotted on to Hybond-ECL nitro-cellulose membranes (GE Healthcare). The membranes were then incubated with the anti-pentaHis mouse monoclonal antibody (Qiagen) at a 1:2000 dilution, and visualized using goat anti-mouse IgG/IgM peroxidase-linked secondary antibody (Jackson ImmunoResearch) at a 1:5000 dilution. After extensive washing, bound antibodies were detected by adding a substrate solution including 3,3'-diaminobenzidine tetrahydrochloride (Sigma) and hydrogen peroxide. Endoproteinase Glu-C digested products were blotted to polyvinylidene difluoride (PVDF) membranes (Millipore) and N-terminal sequencing data were obtained on a Procise protein micro-sequencer (Applied Biosystems) at the Caltech Protein/Peptide Microanalysis Lab (PPMAL). To determine which fragments retained binding to HJV, an HJV affinity column was constructed by coupling several milligrams of HJV to CNBr-activated Sepharose 4B (GE Healthcare) following the manufacturer's instructions.

SPR-based affinity measurements

A BIACORE 2000 or T100 biosensor system (Biacore AB) was used to assay the interactions between HJV, neogenin, and BMP-2 proteins at 25°C in 20 mM HEPES pH 7.4, 150 mM NaCl, 2 mM EDTA and 0.005% surfactant P20 (v/v). Potential aggregates were removed by running protein samples over size exclusion columns immediately before the experiments. Protein concentrations were determined using molar extinction coefficients calculated based on their amino acid sequences using the Expasy ProtParam tool (30). HJV was immobilized on a CM5 chip (research grade, Biacore AB) using standard primary amine coupling chemistry (BIACORE manual) at densities of several hundred resonance units (RUs). In some experiments, the non-cleavable HJV mutant D172A was coupled on an adjacent flow cell. For kinetics-based experiments, complications due to mass transport (31) were avoided by injecting dilutions of various versions of neogenin over the flow cells at flow rates of 50 μl/min or 70 μl/min, which were chosen based on the results of flow rate tests to assess mass transport. HJV-coupled chips were regenerated by three pulses of 100 μl of 2 M $MgCl_2$ when needed. Due to a loss of activity of immobilized HJV, different pairs of interactions were conducted on different sensor chips. Raw sensorgrams were pre-processed using the Scrubber software package (http://www.cores.utah.edu/interaction/scrubber.html). The on- and off-rates, k_a and k_d, were obtained by simultaneous fitting of the association and dissociation phases of all curves in the working set to a 1:1 binding model using the program Clamp99 (32). K_D values were calculated as k_d/k_a.

The affinity of BMP-2 for HJV was derived using an equilibrium-based binding assay in which binding reactions were allowed to reach equilibrium by using slow flow rates (1 – 5 μl/min). HJV was injected at various concentrations over immobilized BMP-2 (coupling density ~790 RU), which was coupled as described for HJV. In some experiments HJV was injected in the presence of 4 μM FNIII 5-6. The binding response at equilibrium (R_{eq}) was plotted as a function of HJV concentration, and best fit binding curves and K_D values were derived by non-linear regression analysis using MATLAB (v7.4, The MathWorks). In the competition experiments in which HJV was injected together with 4 μM FNIII 5-6, residual association between FNIII 5-6 and the BMP-2 chip was accounted for by subtracting the signal obtained by injecting 4 μM FNIII 5-6 in the absence of HJV over the BMP-2 chip (172 RU, whereas 109RU was observed in blank flow cell). The competition assay was repeated using a lower concentration of FNIII 5-6, at which no residual association was observed between FNIII 5-6 and the BMP-2 chip. In this experiment, 500 nM HJV, 400nM FNIII 5-6, or 500 nM HJV plus 400 nM FNIII 5-6 was injected over the BMP-2 chip.

Determination of oligomeric states of proteins and protein-protein complexes

The oligomeric states of HJV and neogenin sFNIII 5-6 were determined by size exclusion chromatography with in-line static light scattering and refractive index monitoring using the ÄKTA chromatography system (GE Healthcare) equipped with a DAWN HELEOS multi-angle light scattering detector and Optilab rEX refractometer (Wyatt Technology Corp.). Purified HJV, neogenin sFNIII 5-6, or a 1:1 mixture of HJV plus neogenin sFNIII 5-6 were run over a Superdex 75 10/30 column (GE Healthcare) in 10 mM Tris pH 8.0, 300 mM NaCl, 5 mM EDTA. Bovine serum albumin (BSA, gel filtration calibration kit from GE Healthcare) was used as a calibration standard. Data were interpreted using the ASTRA V software (Wyatt Technology Corp.).

Oligomeric states were verified by sedimentation velocity analytical ultracentrifugation using an Optima XL-I analytical ultracentrifuge with an An60 Ti four-hole rotor (Beckman Coulter). 440 μl blank buffer and 420 μl filtered protein sample were filled into a standard double-sector centerpiece with sapphire windows and spun at 50,000 rpm. Absorbance data were collected at 280 nm in the continuous mode with radial increments of 0.03 cm. Buffer properties and the partial specific volume for each protein were calculated by SEDNTERP (33). The meniscus and bottom of each set of data were assigned independently using the program SEDFIT (34), which also fits the data to a *c(s)* distribution with the sedimentation coefficient as the x-axis or a c*(M)* distribution plotted against molecular weight (MW).

Results

Production and purification of HJV and neogenin proteins

The ectodomain of HJV was expressed as a soluble protein in baculovirus-infected insect cells. Purified wt HJV migrated as three bands with apparent molecular masses of 40 kDa, 26 kDa, and 14 kDa on reducing SDS-PAGE (Figure 1A, lane 2), similar to the partial cleavage pattern observed for HJV existing in natural sources (16). The 40 kDa band corresponds to the intact protein while the two lower molecular weight bands represent fragments resulting from an auto-cleavage at the D172-P173 bond (16, 17). These fragments are normally linked by disulfide bond(s) (16), as verified by SDS-PAGE analysis under non-reducing conditions (Figure 1B). To produce a homogeneous form of HJV that does not undergo auto-cleavage, we generated a mutant in which Asp172 at the cleavage site was mutated to alanine (HJV D172A). Purified HJV D172A mutant migrated as a single band with an apparent molecular mass of 40 kDa on reducing SDS-PAGE (Figure 1A, lane 3).

Several forms of neogenin were expressed as described in **Experimental Procedures**: the full-length ectodomain, the FNIII domains only (FNIII 1-6), FNIII domains 5 and 6 (in two forms, FNIII 5-6 and the shorter sFNIII 5-6), FNIII domain 5 only (FNIII 5 and sFNIII 5), and FNIII domain 6 only (FNIII 6 and sFNIII 6). With the exception of neogenin FNIII 6 and sFNIII 6, the neogenin sequences all included potential N-linked glycosylation sites, accounting for their migration as multiple closely-spaced bands when analyzed by SDS-PAGE (Figure 1A, lane 4-11).

Neogenin FNIII 1-6 and the full-length neogenin ectodomain bind HJV equally well

The FNIII repeats of neogenin have been shown to be the binding site for chicken RGM (14), a homolog of HJV. In order to determine if the HJV binding site on neogenin also involved the FNIII repeats, we determined binding affinities for the interaction between HJV and intact neogenin versus FNIII 1-6 using a surface plasmon resonance assay. Affinities were determined from the ratios of kinetic constants derived using a 1:1 binding model (Table 1;Figure 2A, B). The affinities for the neogenin/HJV and FNIII 1-6/HJV interactions were both ~500 nM (Table 1), thus the four Ig-like domains of neogenin were unlikely to be involved in

the binding interaction. A higher affinity (9 nM) was reported for the binding of chicken RGM to the ectodomain of chicken neogenin (14), suggesting that HJV relatives in other vertebrate species bind more tightly to neogenin than observed for the interaction between human HJV and human neogenin.

Both intact neogenin and FNIII 1-6 also bound to immobilized HJV D172A (Table 1). In addition, when saturated with excess neogenin, immobilized wt HJV (a mixture of intact and cleaved protein) showed the same maximum response as a function of coupling density as immobilized non-cleavable HJV D172A, suggesting that neogenin binds to both cleaved and uncleaved forms of HJV and rationalizing why only a single affinity was required to describe the wt HJV interaction with intact neogenin and FNIII 1-6.

HJV binds to a proteolytic fragment of neogenin including the two C-terminal FNIII domains

Neogenin is a member of a family of monomeric cell surface proteins with flexible and extended ectodomains that contain multiple Ig and FNIII domains arranged in tandem (35). Consistent with an extended structure for neogenin and FNIII 1-6, both proteins migrated with larger apparent molecular weights than corresponding globular proteins when analyzed by gel filtration chromatography (Figure 1C). Reasoning that HJV is unlikely to contact all six domains in an extended FNIII 1-6 structure, we subjected purified FNIII 1-6 to treatment with various proteases in order to find smaller stable fragments and test them for binding to HJV. Endoproteinase Glu-C digestion gave rise to two major proteolytic products, while other proteases either generated many fragments (trypsin, papain, and thermolysin) or did not cleave FNIII 1-6 (thrombin), as assayed by SDS-PAGE (Supporting Information Figure S1A). The two endoproteinase Glu-C-produced fragments migrated with apparent molecular masses of 45 kDa and 30 kDa in reducing SDS-PAGE. Western blotting using an anti-poly-His antibody showed that the smaller fragment retained the C-terminal 6x-His tag, thus representing a C-terminal fragment of neogenin FNIII 1-6 (Supporting Information Figure S1B). By using HJV-coupled Sepharose beads in a pull-down assay followed by SDS-PAGE, we found that only the smaller fragment showed detectable binding to HJV (Supporting Information Figure S1C). N-terminal sequencing of the smaller fragment revealed the sequence VDLFVI, which uniquely identified the cleavage site to be after a glutamate residue located at the end of fourth FNIII domain. These results localized the HJV-binding site to FNIII 5, FNIII 6 and/or the residues C-terminal to FNIII 6.

Neogenin FNIII 5-6 binds tightly to HJV with critical interactions contributed by FNIII 6

To further characterize the HJV-binding epitope on neogenin, we expressed FNIII 5-6, a recombinant form of the HJV-binding proteolytic fragment produced from FNIII 1-6. The affinity obtained for neogenin FNIII 5-6 binding to immobilized wt HJV was higher than the affinity obtained for intact neogenin, with a K_D in the sub-nanomolar range (Figure 2C).

To further map the HJV binding site on FNIII 5-6, we tested the binding of single domain constructs, FNIII 5 and FNIII 6, to HJV. No binding to immobilized HJV was observed at concentrations up to 8 μM for FNIII 5, whereas FNIII 6 bound to HJV with an affinity of ~20 nM (Figure 2D), which is ~100-fold weaker than the affinity of FNIII 5-6, but 25-fold stronger than the affinity of FNIII 1-6. These results suggest that the HJV-binding epitope is primarily located on FNIII 6, with minor contributions from the hinge region between FNIII 5 and 6 and/ or from FNIII 5.

The C-terminal linking region of the neogenin ectodomain contributes to HJV binding

Unlike other Ig superfamily cell surface receptors such as L1 (36), neogenin contains a long linking region (42 residues) between the end of the last FNIII domain and the beginning of the transmembrane region. The sequence is highly conserved among neogenins from different

species including human, mouse, rat and chicken, but no significant similarities were found to any other known proteins by searching in the NCBI database. To determine the effects of this linking region on binding to HJV, we compared the affinities of neogenin FNIII constructs with and without the linking region. The binding of two forms of neogenin FNIII domains lacking the linking region (sFNIII 5-6 and sFNIII 6) to HJV was compared to the binding of two forms containing the linking region (FNIII 5-6 and FNIII 6). In both cases, the forms containing the C-terminal tail bound 10-100 fold more tightly to HJV than the shorter forms lacking the tail (Figure 2 and Table 1).

HJV and neogenin are monomers that form a 1:1 complex

We used in-line static multi-angle light scattering and analytical ultracentrifugation to determine the oligomeric states of sFNIII 5-6, HJV, and their complex (Figure 3). As shown in Figure 3A and B, sFNIII 5-6 and HJV were monomers based on a comparison of their molecular masses calculated from their amino acid sequences (23.9 kDa and 39.8 kDa, not including N-linked glycans) with experimentally-determined molecular masses derived from multi-angle light scattering data (24.4 kDa and 47.8 kDa). A comparable light-scattering experiment demonstrated that the neogenin FNIII 1-6 domain construct was also monomeric (Supporting Information Figure 2). The molecular weights of the sFNIII 5-6 and HJV proteins were also derived by sedimentation velocity analytical ultracentrifugation (Figure 3D, E), yielding single peaks centered at 27 kDa (sFNIII 5-6) and 42 kDa (HJV) in a mass distribution plot (Figure 3F), consistent with the results obtained by multi-angle light scattering.

To determine the stoichiometry of the HJV/sFNIII 5-6 complex, we repeated the in-line multi-angle light scattering experiment by running a 1:1 mixture of HJV and sFNIII 5-6 over the size exclusion column. Only one peak was found in the column profile for the mixture (Figure 3C). The average molecular weight determined for this peak was 70.7 kDa, indicating that the complex was formed at a molar ratio of one HJV to one sFNIII 5-6. These results rule out avidity effects resulting from multimerization of sFNIII 5-6 as an explanation for its tight binding to HJV (Figure 2) and justify the use of 1:1 binding models for fitting the biosensor binding data.

BMP-2 and neogenin bind to non-overlapping sites on HJV

To determine the effects of BMP-2 on the binding of HJV to neogenin, we first determined the affinity of HJV for BMP-2. Using an equilibrium-based biosensor binding assay in which HJV was injected over immobilized BMP-2, the affinity was derived as ~140 nM (Figure 4A), ~30-50-fold weaker than the affinities reported in pervious studies involving interactions between various RGM-Fc fusion proteins and immobilized BMP-2 (27, 37). The higher affinities reported previously are likely to be due to avidity effects resulting from cross-linking of the bivalent RGM-Fc fusion protein to immobilized BMP-2 dimer. Given that HJV is not normally dimeric (Figure 3B), the lower affinity derived in the present studies is relevant to the physiological situation in which monomeric HJV interacts with BMP-2.

We next repeated the HJV/BMP-2 binding assay in the presence of a saturating concentration (4 μM) of FNIII 5-6. After subtracting the residual response due to injecting a high concentration of FNIII 5-6 over the BMP-2 surface, we observed a higher maximal binding response for HJV in the presence of FNIII 5-6 than in its absence, but no significant change in the derived affinity (K_D = 67 nM) (Figure 4A). This result suggested that an FNIII 5-6/HJV complex was binding to immobilized BMP-2, implying that FNIII 5-6 and BMP-2 bind to non-overlapping sites on HJV.

To verify that neogenin and BMP-2 can bind simultaneously to HJV, we repeated the competition binding experiment using a lower concentration of FNIII 5-6, so that there was no

detectable interaction between FNIII 5-6 and the BMP-2 surface. In this experiment, 500 nM HJV was injected in the presence and absence of 400 nM neogenin FNIII 5-6 over immobilized BMP-2. As expected, HJV bound to the BMP-2 surface, but no binding was observed when FNIII 5-6 was injected over immobilized BMP-2 (Figure 4B). Next, a mixture of HJV and neogenin FNIII 5-6 was injected over the same BMP-2 surface. A higher maximum response was observed for the binding of the FNIII 5-6/HJV mixture to immobilized BMP-2 (Figure 4B, the third injection) than for the binding of HJV alone (Figure 4B, the first injection). Since neogenin FNIII 5-6 did not bind BMP-2 directly, the signal increase resulted from an FNIII 5-6/HJV complex binding to immobilized BMP-2 via the HJV protein, demonstrating that BMP-2 and neogenin can bind simultaneously to non-overlapping sites on HJV to form a ternary complex.

Discussion

HJV is an iron-regulatory protein primarily expressed in skeletal muscle and liver that functions as an upstream modulator of the expression of hepcidin, a liver-synthesized peptide responsible for regulating iron levels in mammals (12). How the body iron status affects HJV and how HJV in turn regulates hepcidin expression is unclear. Recent work suggests a two-step process by which serum iron status, as determined by the concentration of iron-loaded transferrin, modulates hepcidin expression as follows: 1) low iron-loaded transferrin levels cause increased neogenin-mediated HJV shedding (28), resulting in increased serum HJV and reduced membrane-bound HJV on hepatocytes, and 2) soluble HJV binds to BMP-2 in the blood, preventing its binding to cell surface receptors, thereby reducing BMP signaling and hepcidin expression in hepatocytes (26).

Here we used a biochemical approach to characterize the interactions between HJV, neogenin and BMP-2. We focused initially on the neogenin-HJV interaction, finding that HJV binds to the membrane-proximal region of neogenin, an extended protein with 10 extracellular domains. This finding is of interest given that HJV and its RGM relatives can engage in both *cis* (on the same cell) and *trans* (between cells) interactions with neogenin. For example, neogenin/RGM interactions in axon guidance occur in *trans* (38), whereas the HJV/neogenin interaction on muscle cells probably occurs in *cis*. Assuming similar binding of neogenin by HJV and the RGMs, which are closely related by sequence to HJV (12), HJV and/or RGMs would be required to access the membrane-proximal region of neogenin whether the proteins are bound to the same or different cells, implying flexibility in one or both of the binding partners. During a *cis* interaction between HJV and neogenin on muscle cells, membrane-bound HJV may be required to bend over to access its binding epitope on the membrane-proximal FNIII 5-6 domains, thereby possibly exposing it to cleavage. Thus the mapping of the HJV binding epitope on neogenin to its most membrane-proximal domain may help explain the correlation between neogenin binding and HJV shedding (28).

We also discovered that HJV bound to the C-terminal extracellular domains of neogenin 2-3 orders of magnitude more tightly than to the entire neogenin ectodomain. This affinity difference was consistent with differences in the concentrations of each protein required to inhibit HJV shedding from cells expressing intact neogenin and HJV proteins (An-Sheng Zhang and Caroline A. Enns, personal communication). One mechanism to account for the affinity difference is that HJV binds preferentially to an HJV-accessible conformation of neogenin (mimicked by the FNIII 5-6 protein) that is in equilibrium with a non-accessible conformation, and that addition of HJV shifts the equilibrium to favor the accessible conformation. This model predicts that HJV would bind to the entire neogenin ectodomain with a slower association rate than it binds to FNIII 5-6, while the dissociation rates would be similar. These predictions are consistent with the kinetic data in Table 1, in which it is shown

that the association rate for the intact neogenin ectodomain was two orders of magnitude lower than that for FNIII 5-6, while the dissociation rates were similar.

Although mutations in HJV in juvenile hemochromatosis patients and deletion of HJV in mice resulted in abnormally low hepcidin expression (20), it is unlikely that the interaction between HJV and neogenin is directly involved in regulating hepcidin levels. Instead, recent findings demonstrating that HJV binds some BMPs and that incubation of hepatocytes with exogenous BMP-2 upregulates hepcidin expression (26) suggest a more direct role for the HJV-BMP interaction in regulating hepcidin. The BMP signaling pathway is activated by the binding of BMPs to the type II and type I BMP receptor kinases, which in turn induces Smad activation and nuclear translocation, resulting in ligand-specific transcription (39). Membrane-bound HJV has been shown to act as a BMP co-receptor (26), thus complexes of BMP with its classic receptors and with HJV are likely to exist on the hepatocyte membrane. Here we show that BMP-2 and neogenin could bind simultaneously to HJV, consistent with previous observations that neither BMP-2 nor its antagonist noggin affects neogenin-mediated HJV-shedding (28). Thus the possibility that neogenin is a component in a cell surface complex that includes BMP receptors, HJV, and BMP must be considered in models for how BMP and HJV affect hepcidin levels to regulate iron homeostasis.

Supplementary Material

Refer to Web version on PubMed Central for supplementary material.

Acknowledgments

The abbreviations used are

AU	absorbance unit
BMP	bone morphogenetic protein
CNBr	cyanogen bromide
FNIII	fibronectin type III
HEPES	4-(2-Hydroxyethyl) piperzine-1-ethanesulfonic acid
HJV	hemojuvelin
Ig	immunoglobulin
JH	juvenile hemochromatosis
MW	molecular weight
NTA	nitrilotriacetic acid
RGM	repulsive guidance molecule
RU	resonance unit
SPR	surface plasmon resonance
Tris	Tris (hydroxymethyl) aminomethane
UV	ultraviolet

wt   wildtype

References

1. Hentze MW, Muckenthaler MU, Andrews NC. Balancing acts: molecular control of mammalian iron metabolism. Cell 2004;117:285–297. [PubMed: 15109490]

2. Dautry-Varsat A, Ciechanover A, Lodish HF. pH and the recycling of transferrin during receptor-mediated endocytosis. Proc Natl Acad Sci U S A 1983;80:2258–2262. [PubMed: 6300903]

3. Feder JN, Gnirke A, Thomas W, Tsuchihashi Z, Ruddy DA, Basava A, Dormishian F, Domingo R Jr. Ellis MC, Fullan A, Hinton LM, Jones NL, Kimmel BE, Kronmal GS, Lauer P, Lee VK, Loeb DB, Mapa FA, McClelland E, Meyer NC, Mintier GA, Moeller N, Moore T, Morikang E, Prass CE, Quintana L, Starnes SM, Schatzman RC, Brunke KJ, Drayna DT, Risch NJ, Bacon BR, Wolff RK. A novel MHC class I-like gene is mutated in patients with hereditary haemochromatosis. Nat Genet 1996;13:399–408. [PubMed: 8696333]

4. Camaschella C, Roetto A, Cali A, De Gobbi M, Garozzo G, Carella M, Majorano N, Totaro A, Gasparini P. The gene TFR2 is mutated in a new type of haemochromatosis mapping to 7q22. Nat Genet 2000;25:14–15. [PubMed: 10802645]

5. Abboud S, Haile DJ. A novel mammalian iron-regulated protein involved in intracellular iron metabolism. J Biol Chem 2000;275:19906–19912. [PubMed: 10747949]

6. Donovan A, Brownlie A, Zhou Y, Shepard J, Pratt SJ, Moynihan J, Paw BH, Drejer A, Barut B, Zapata A, Law TC, Brugnara C, Lux SE, Pinkus GS, Pinkus JL, Kingsley PD, Palis J, Fleming MD, Andrews NC, Zon LI. Positional cloning of zebrafish ferroportin1 identifies a conserved vertebrate iron exporter. Nature 2000;403:776–781. [PubMed: 10693807]

7. McKie AT, Marciani P, Rolfs A, Brennan K, Wehr K, Barrow D, Miret S, Bomford A, Peters TJ, Farzaneh F, Hediger MA, Hentze MW, Simpson RJ. A novel duodenal iron-regulated transporter, IREG1, implicated in the basolateral transfer of iron to the circulation. Mol Cell 2000;5:299–309. [PubMed: 10882071]

8. Njajou OT, Vaessen N, Joosse M, Berghuis B, van Dongen JW, Breuning MH, Snijders PJ, Rutten WP, Sandkuijl LA, Oostra BA, van Duijn CM, Heutink P. A mutation in SLC11A3 is associated with autosomal dominant hemochromatosis. Nat Genet 2001;28:213–214. [PubMed: 11431687]

9. Krause A, Neitz S, Magert HJ, Schulz A, Forssmann WG, Schulz-Knappe P, Adermann K. LEAP-1, a novel highly disulfide-bonded human peptide, exhibits antimicrobial activity. FEBS Lett 2000;480:147–150. [PubMed: 11034317]

10. Park CH, Valore EV, Waring AJ, Ganz T. Hepcidin, a urinary antimicrobial peptide synthesized in the liver. J Biol Chem 2001;276:7806–7810. [PubMed: 11113131]

11. Roetto A, Papanikolaou G, Politou M, Alberti F, Girelli D, Christakis J, Loukopoulos D, Camaschella C. Mutant antimicrobial peptide hepcidin is associated with severe juvenile hemochromatosis. Nat Genet 2003;33:21–22. [PubMed: 12469120]

12. Papanikolaou G, Samuels ME, Ludwig EH, MacDonald ML, Franchini PL, Dube MP, Andres L, MacFarlane J, Sakellaropoulos N, Politou M, Nemeth E, Thompson J, Risler JK, Zaborowska C, Babakaiff R, Radomski CC, Pape TD, Davidas O, Christakis J, Brissot P, Lockitch G, Ganz T, Hayden MR, Goldberg YP. Mutations in HFE2 cause iron overload in chromosome 1q-linked juvenile hemochromatosis. Nat Genet 2004;36:77–82. [PubMed: 14647275]

13. Franchini M, Veneri D. Recent advances in hereditary hemochromatosis. Ann Hematol 2005;84:347–352. [PubMed: 15747119]

14. Rajagopalan S, Deitinghoff L, Davis D, Conrad S, Skutella T, Chedotal A, Mueller BK, Strittmatter SM. Neogenin mediates the action of repulsive guidance molecule. Nat Cell Biol 2004;6:756–762. [PubMed: 15258590]

15. Matsunaga E, Chedotal A. Repulsive guidance molecule/neogenin: a novel ligand-receptor system playing multiple roles in neural development. Dev Growth Differ 2004;46:481–486. [PubMed: 15610137]

16. Lin L, Goldberg YP, Ganz T. Competitive regulation of hepcidin mRNA by soluble and cell-associated hemojuvelin. Blood 2005;106:2884–2889. [PubMed: 15998830]

17. Zhang AS, West AP Jr. Wyman AE, Bjorkman PJ, Enns CA. Interaction of hemojuvelin with neogenin results in iron accumulation in human embryonic kidney 293 cells. J Biol Chem 2005;280:33885–33894. [PubMed: 16103117]

18. Lin L, Nemeth E, Goodnough JB, Thapa DR, Gabayan V, Ganz T. Soluble hemojuvelin is released by proprotein convertase-mediated cleavage at a conserved polybasic RNRR site. Blood Cells Mol Dis 2008;40:122–131. [PubMed: 17869549]

19. Lanzara C, Roetto A, Daraio F, Rivard S, Ficarella R, Simard H, Cox TM, Cazzola M, Piperno A, Gimenez-Roqueplo AP, Grammatico P, Volinia S, Gasparini P, Camaschella C. Spectrum of hemojuvelin gene mutations in 1q-linked juvenile hemochromatosis. Blood 2004;103:4317–4321. [PubMed: 14982873]

20. Huang FW, Pinkus JL, Pinkus GS, Fleming MD, Andrews NC. A mouse model of juvenile hemochromatosis. J Clin Invest 2005;115:2187–2191. [PubMed: 16075059]

21. Vielmetter J, Chen XN, Miskevich F, Lane RP, Yamakawa K, Korenberg JR, Dreyer WJ. Molecular characterization of human neogenin, a DCC-related protein, and the mapping of its gene (NEO1) to chromosomal position 15q22.3-q23. Genomics 1997;41:414–21. [PubMed: 9169140]

22. Meyerhardt JA, Look AT, Bigner SH, Fearon ER. Identification and characterization of neogenin, a DCC-related gene. Oncogene 1997;14:1129–1136. [PubMed: 9121761]

23. Matsunaga E, Tauszig-Delamasure S, Monnier PP, Mueller BK, Strittmatter SM, Mehlen P, Chedotal A. RGM and its receptor neogenin regulate neuronal survival. Nat Cell Biol 2004;6:749–755. [PubMed: 15258591]

24. Chen D, Zhao M, Mundy GR. Bone morphogenetic proteins. Growth Factors 2004;22:233–241. [PubMed: 15621726]

25. Wagner TU. Bone morphogenetic protein signaling in stem cells--one signal, many consequences. Febs J 2007;274:2968–2976. [PubMed: 17521338]

26. Babitt JL, Huang FW, Wrighting DM, Xia Y, Sidis Y, Samad TA, Campagna JA, Chung RT, Schneyer AL, Woolf CJ, Andrews NC, Lin HY. Bone morphogenetic protein signaling by hemojuvelin regulates hepcidin expression. Nat Genet 2006;38:531–539. [PubMed: 16604073]

27. Xia Y, Yu PB, Sidis Y, Beppu H, Bloch KD, Schneyer AL, Lin HY. Repulsive guidance molecule RGMa alters utilization of bone morphogenetic protein (BMP) type II receptors by BMP2 and BMP4. J Biol Chem 2007;282:18129–18140. [PubMed: 17472960]

28. Zhang AS, Anderson SA, Meyers KR, Hernandez C, Eisenstein RS, Enns CA. Evidence that inhibition of hemojuvelin shedding in response to iron is mediated through neogenin. J Biol Chem 2007;282:12547–12556. [PubMed: 17331953]

29. Allendorph GP, Vale WW, Choe S. Structure of the ternary signaling complex of a TGF-beta superfamily member. Proc Natl Acad Sci U S A 2006;103:7643–7648. [PubMed: 16672363]

30. Gill SC, von Hippel PH. Calculation of protein extinction coefficients from amino acid sequence data. Anal Biochem 1989;182:319–326. [PubMed: 2610349]

31. Schuck P. Kinetics of ligand binding to receptor immobilized in a polymer matrix, as detected with an evanescent wave biosensor. I. A computer simulation of the influence of mass transport. Biophys J 1996;70:1230–1249. [PubMed: 8785280]

32. Morton TA, Myszka DG. Kinetic analysis of macromolecular interactions using surface plasmon resonance biosensors. Methods Enzymol 1998;295:268–294. [PubMed: 9750223]

33. Laue TM, B. D. S. Ridgeway TM, Pelletier SL. Harding SE, Rowe AJ, Horton JC. Computer-aided interpretation of analytical sedimentation data for proteins. Analytical Ultracentrifugation in Biochemistry and Polymer Science 1992:90–125.

34. Schuck P. Size-distribution analysis of macromolecules by sedimentation velocity ultracentrifugation and lamm equation modeling. Biophys J 2000;78:1606–1619. [PubMed: 10692345]

35. Kasper C, Rasmussen H, Kastrup JS, Ikemizu S, Jones EY, Berezin V, Bock E, Larsen IK. Structural basis of cell-cell adhesion by NCAM. Nat Struct Biol 2000;7:389–393. [PubMed: 10802736]

36. Bateman A, Jouet M, MacFarlane J, Du JS, Kenwrick S, Chothia C. Outline structure of the human L1 cell adhesion molecule and the sites where mutations cause neurological disorders. Embo J 1996;15:6050–6059. [PubMed: 8947027]

37. Halbrooks PJ, Ding R, Wozney JM, Bain G. Role of RGM coreceptors in bone morphogenetic protein signaling. J Mol Signal 2007;2:4. [PubMed: 17615080]

38. Yamashita T, Mueller BK, Hata K. Neogenin and repulsive guidance molecule signaling in the central nervous system. Curr Opin Neurobiol 2007;17:29–34. [PubMed: 17169551]

39. Derynck R, Zhang YE. Smad-dependent and Smad-independent pathways in TGF-beta family signalling. Nature 2003;425:577–584. [PubMed: 14534577]
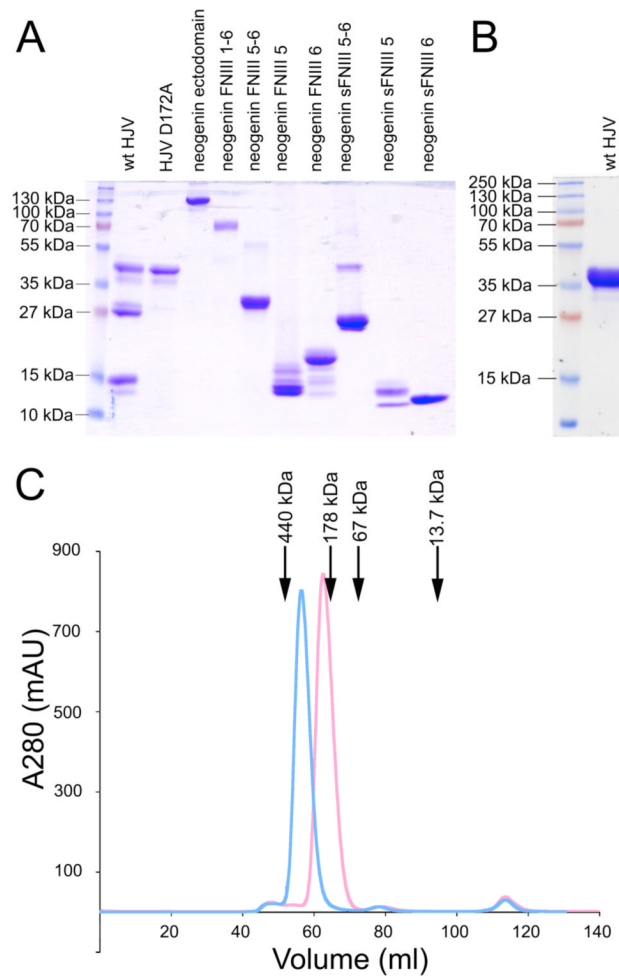
Figure 1. Characterizations of HJV and neogenin proteins
(A) Purified HJV and neogenin proteins were separated by 13% reduced SDS-PAGE and stained with Coomassie blue. Molecular weights of standard proteins are indicated on the left. (B) Purified wt HJV analyzed by 13% non-reduced SDS-PAGE. (C) Size exclusion chromatography traces of the neogenin ectodomain (cyan) and neogenin FNIII 1-6 (pink) with absorbance at 280 nm (in absorbance unit, AU) plotted against retention volume (in ml). From left to right, black arrows point to the retention volumes of molecular weight standards: ferritin (440 kDa, 53.0 ml), aldolase (158 kDa, 65.0 ml), albumin (67 kDa, 72.7 ml), and ribonuclease A (13.7 kDa, 95.1 ml).
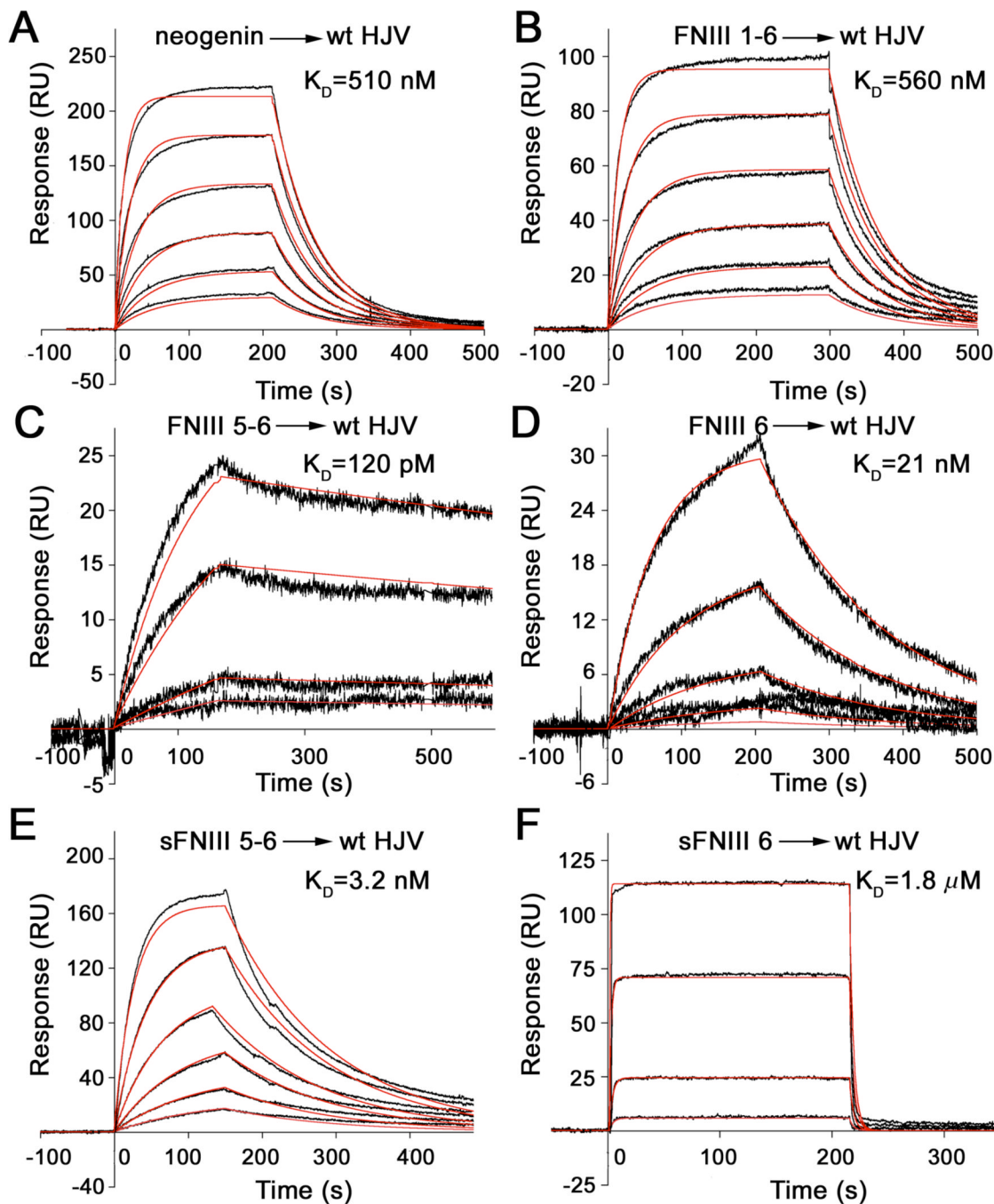
Figure 2. Representative SPR data for neogenin proteins binding to immobilized wildtype HJV
In each panel, the protein that was injected over immobilized wt HJV is indicated before the arrow. Proteins were injected as a series of 2-fold dilutions, with the highest injected concentrations being 2 μM, 2 μM, 1.2 nM, 40 nM, 20 nM, and 10 μM, for panels A-F, respectively. Sensorgrams (black lines) are overlaid with the simulated response (red lines) derived using a 1:1 binding model. The K_D values shown in each panel are the calculated affinities for the single experiment shown, whereas Table 1 reports average values derived from multiple experiments.
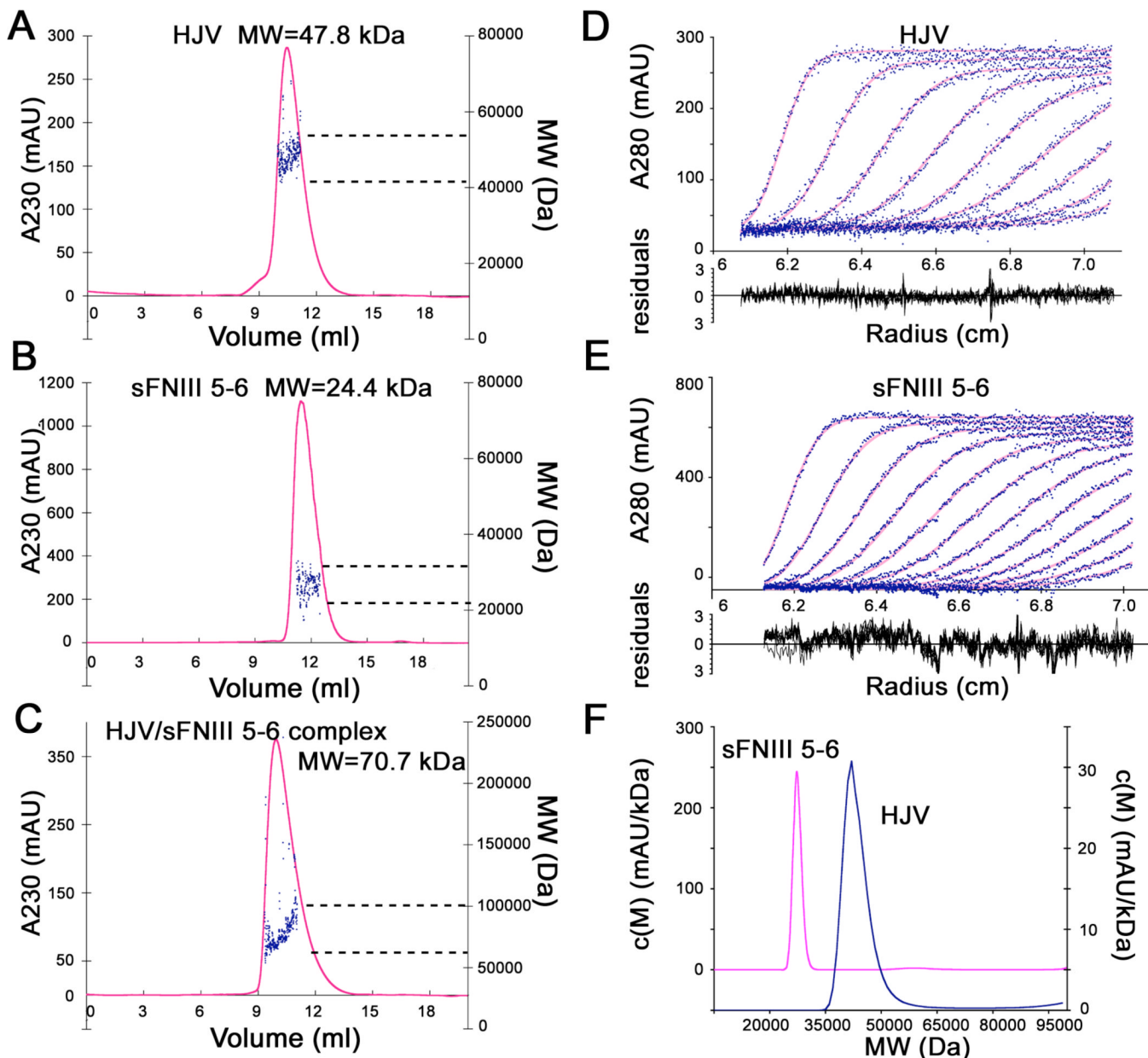
Figure 3. Multi-angle light scattering and sedimentation velocity analytical ultracentrifugation experiments to determine the oligomeric states of sFNIII 5-6 and HJV

(A-C) Multi-angle light scattering data were obtained by injecting protein samples into a size exclusion chromatography system with in-line light scattering and refractive index monitors. Traces of UV absorbance at 230 nm are shown as continuous pink lines. Calculated molecular weights based on multi-angle light scattering data are indicated as blue dots with units shown on the right axis. (A) wt HJV. (B) neogenin sFNIII 5-6. (C) HJV/sFNIII 5-6 complex. (D-F) Sedimentation velocity analytical ultracentrifugation data. (D-E) Sedimentation velocity scans of the absorbance distributions (blue dots) collected for wt HJV (panel D) and neogenin sFNIII 5-6 (panel E), and their best-fit modeled curves (pink continuous line) generated by SEDFIT. Residuals are shown below the curves in black. For clarity, only one out of every ten scans were included in the plots although all scans were used in modeling. (F) Derived molecular weight distributions for wt HJV (blue line, with units shown on right axis) and neogenin sFNIII

5-6 (pink line, with units shown on left axis). c(M) is the unnormalized probability density function of molecular weight and the integration of c(M) over molecular weight equals to the absorbance of the protein sample.
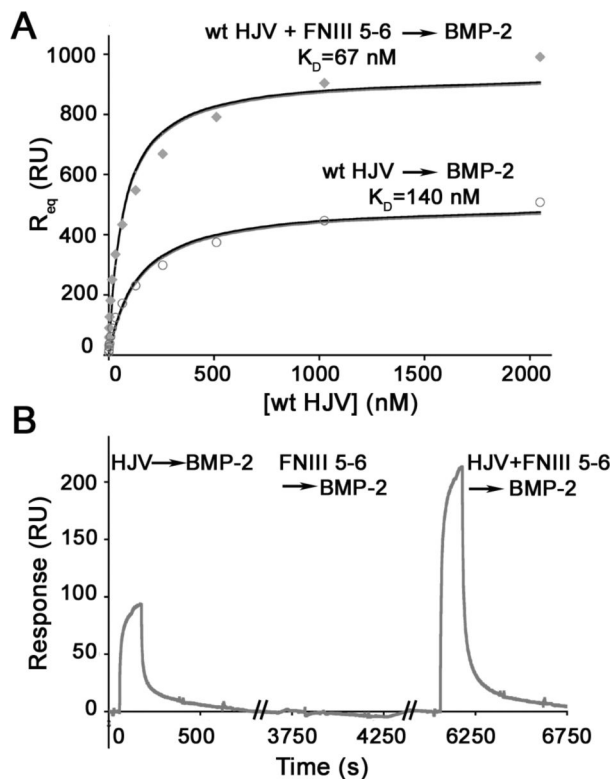
Figure 4. Neogenin FNIII 5-6 and BMP-2 do not compete for HJV binding

(A) Plots of equilibrium binding response (R_{eq}) versus the concentration of injected HJV. BMP-2 was immobilized on a sensor chip, and different concentrations of wt HJV were injected in the absence (hollow circles) or presence (solid diamonds) of a saturating concentration (4 μM) of FNIII 5-6. Best fit binding curves (continuous lines) and K_D values were derived by non-linear regression analysis. K_D values obtained from an independently-conducted experiment using a different BMP-2-coupled flow cell were 130 nM in the absence of FNIII 5-6 and 59 nM in the presence of FNIII 5-6. (B) Sensorgrams from injections of HJV, FNIII 5-6, or their complex over immobilized BMP-2. Left: Injection of 500 nM HJV. Middle: Injection of 400 nM neogenin FNIII 5-6. Right: Injection of a mixture of 500 nM HJV and 400 nM neogenin FNIII 5-6.

Table 1

SPR analyses of the binding of neogenin proteins to immobilized HJV

	K_D (M)	k_a (M^{-1}sec^{-1})	k_d (sec^{-1})
neogenin ectodomain → wt HJV	$(5.1, 5.0) \times 10^{-7}$	$(2.5, 3.3) \times 10^4$	$(1.3, 1.6) \times 10^{-2}$
neogenin FNIII 1-6 → wt HJV	$(5.6, 5.3) \times 10^{-7}$	$(2.3, 2.7) \times 10^4$	$(1.3, 1.4) \times 10^{-2}$
neogenin FNIII 5-6 → wt HJV	$(2.2 \pm 1.5) \times 10^{-10}$	$(4.7 \pm 2.0) \times 10^6$	$(1.0 \pm 0.7) \times 10^{-3}$
neogenin FNIII 5th → wt HJV	NB		
neogenin FNIII 6th → wt HJV	$(1.8, 2.1) \times 10^{-8}$	$(3.1, 2.8) \times 10^5$	$(5.6, 5.9) \times 10^{-3}$
neogenin sFNIII 5-6 → wt HJV	$(3.6 \pm 0.6) \times 10^{-9}$	$(2.3 \pm 0.6) \times 10^6$	$(8.0 \pm 1.1) \times 10^{-3}$
neogenin sFNIII 5th → wt HJV	NB		
neogenin sFNIII 6th → wt HJV	$(1.9 \pm 0.08) \times 10^{-6}$	$(1.4 \pm 0.19) \times 10^5$	$(2.6 \pm 0.35) \times 10^{-1}$
neogenin ectodomain → HJV D172A	2.1×10^{-6}	3.0×10^4	6.4×10^{-2}
neogenin FNIII 1-6 → HJV D172A	3.0×10^{-6}	1.3×10^4	3.8×10^{-2}

K_Ds are shown as the average and standard deviation derived from three or four independent measurements, or as one or two K_D values for interactions that were measured in single or duplicate experiments. "NB" indicates that no binding was detected at concentrations up to 8 μM.